

Simulation of Micro-Electroforming for U-Type Micro-Cavity

Sheau-Wen Shiah*, Pai-Yu Chang**, and Po-Hung Lin***

*Department of Naval Architecture and Marine Engineering, Chung Cheng Institute of Technology,
National Defense University

**Department of Product Design, Fortune Institute of Technology

***Graduate School of Defense Science, Chung Cheng Institute of Technology, National Defense University

ABSTRACT

In this study, 0.6 mol/liter CuSO_4 + 1.85 mol/liter H_2SO_4 was used as an electrolyte to achieve micro-electroforming on U-type micro-cavities with various low aspect ratios. A commercial code, CFD-RC, was used to calculate and to obtain the analytic capacity of the micro-cavity for the flowing electrolyte, including the streamline, isoshear-rate, isoconcentration and isovoltage patterns. The mass fractions Sh/Sh_{max} on the surface of the cathode for various parameters $Pe = 1.31 \sim 100$, and for various cavity widths $a = 15 \sim 150 \mu\text{m}$ are determined. For $Pe = 1.31, 41.6$ and $a = 15, 30, 150 \mu\text{m}$, the results indicate excellent consistency with the numerical findings of Kondo and Fukui. The ratio of friction coefficients $C_f/C_{f,max}$ and the current density fraction I/I_{max} for cavities of various widths $a = 15 \sim 150 \mu\text{m}$ satisfied the sagging condition. The current density fraction I/I_{max} can be used to predict that the current density distribution is relatively flat when the cavity width $a = 15 \mu\text{m}$, at which the electroform layer is flatter than at any other cavity width.

Keywords: micro-electroforming, mass fraction, friction coefficient, current density fraction

微電鑄於 U 型微孔穴之數值模擬

夏曉文* 張百禹** 林柏宏***

*國防大學中正理工學院造船系

**和春技術學院商品設計學系

***國防大學中正理工學院國防科學研究所

摘 要

本文採取電鍍液 0.6 mol/l CuSO_4 + 1.85 mol/l H_2SO_4 ，針對不同低深寬比 U 型孔穴進行微電鑄，藉由數值模擬軟體 CFD-RC 使用及計算，獲得微結構 U 型孔穴電鑄物件內電鍍液之流場分佈、剪變率分佈、濃度分佈及電壓分佈之電鍍行為分析。不同的沛克雷數參數效應 $Pe=1.31 \sim 100$ 及不同的幾何孔穴寬度效應 $a = 15 \sim 150 \mu\text{m}$ 分別被探討比較。當 $Pe = 1.31, 41.6$ 以及 $a = 15, 30, 150 \mu\text{m}$ 時，於孔穴陰極面取質量分率 Sh/Sh_{max} ，其結果與 Kondo 及 Fukui 之結果具有一致性。又於不同的孔穴寬度 $a=15 \sim 150 \mu\text{m}$ 取摩擦係數分率 $C_f/C_{f,max}$ 及電流密度分率 I/I_{max} ，其圖形分別皆滿足中垂的現象。由電流密度分率 I/I_{max} 分佈現象，可以預期孔穴寬度 $a = 15 \mu\text{m}$ 分佈曲線所形成的微鑄層外形會較其他不同寬度孔穴鑄層外形平坦。

關鍵字：微電鑄，質量分率，摩擦係數，電流密度分率

文稿收件日期 94.05.30; 文稿修正後接受日期 94.11.21.

Manuscript received May 30, 2005; revised November 21, 2005.

I. INTRODUCTION

The development of technology has advanced to the point where new products are constantly being developed to achieve convenient features, leading to the second generation micro-system technology. Nano-engineering and micro-system technology will be the next major developments in manufacturing technology. These technologies can be integrated with high precision manufacturing and semiconductor technologies and collocated with technologies of synchronous radiation using new materials, modulus and elements, thus, boosting the development of micro-miniaturization, super-precision, high-density, integration and high efficiency technology. Micro-electroforming technology has been successfully applied in various fields, for example, information, communication, optical electronics and biomedicine.

Micro-electroforming includes various behaviors of mechanics, chemistry, electricity, and so on, these behaviors mutually affected one another during electroforming. First, the effect of internal stress, see relevant research by Yang and Kang [1], indicated that the cladding material induces the phenomena of twist and deformation, also used the second cathode to reduce the internal stress in the Ni-cladding process and increase the uniformity of the Ni-cladding material. Savinell et al. [2] examined micro-electroforming and used pulse current to increase the tension and yielding stress for the alloy of Ni-P. Moreover, Tan and Chan [3] used reverse pulse current technology and reduced the internal stress in micro-electroforming for Ni material. Furthermore, the effect of Current

density, DC source is frequently used for micro-electroforming. However, the larger internal stress in the cladding layer causes the surface to be uneven. Using pulse current can boost cladding layer density, increase adhesive force, and reduce internal stress. Lee et al. [4] and Yin et al. [5] used the pulse current for the micro-electroforming of Ni-W alloy, and determined the degree to which the wolfram material is increased by the pulse current. To determine the stirring effect, Andricacos et al. [6] used the ring disk technology for depositing Ni-Fe film in the cathode electrode, increased the convection flow effect, obtained much alloy ion mass diffusion and reduced the proliferation thickness. Furthermore, to measure the current density and the polarization curve on the ring disk. Regarding the influence of electrolyte concentration, cladding layer ability to resist erosion is affected by the electrolyte concentration PH value. Yamasaki et al. [7] noted that chloride ammonium concentration in electrolyte seriously influenced the Ni-W alloys of the cladding layer. When chloride ammonium 0.5 mol/l was taken, the optimum wolfram content in cladding layer was obtained, while an excessive chloride ammonium concentration limited the wolfram content of the cladding layer. Additionally, selecting different electrolyte also can influence the micro-electroforming module. Gould and Lopez [8] conducted sandwich structure electroforming on SiO_x , and found that the gold electrolyte is more stable than aluminum electrolyte.

For the numerical analysis and the discussion of the physical aspects of micro- electroforming

are sourced in the last 20 years. Hessami and Tobias [9] simulated the co-deposit of Ni-Fe alloys, and established diffusion and convection equations. Pesco and Cheh [10] demonstrated that electrolyte mass was only affected by diffusion flow for cavities with a high aspect ratio. However, both diffusion mass flow effect and convection mass flow effect existed when the electrolyte flow was laminar. Kondo et al. [11] described the width of the cavity more 200 μm , the effect of convection mass transfer governs the behavior of the electrolyte for micro-electroforming. However, when cavity width is less 100 μm , the effect of diffusion mass transfer is to dominate. Georgiadou [12] took electrolyte 0.002 mol/l CuSO_4 + 0.1 mol/l H_2SO_4 , and calculated the current density only for the cathode surface. Moreover, Duchanoy and Lopicque [13] displayed that the effect of current density for micro-electroforming altered the angle of the holes, and observed that the lower Reynolds number condition had a more uniform distribution cladding layer than the higher Reynolds number condition.

The literature on the simulation of micro-electroforming is very limited, and the authors are not aware of any study that has disregarded the complete behaviors, including the electrolyte flow distribution, mass transfer distribution, cathode voltage distribution and shear stress distribution in the micro-electroforming process. For this study, electrolyte 0.6 mol/liter CuSO_4 + 1.85 mol/liter H_2SO_4 was taken for micro-electroforming of the U-type micro-cavity. A commercial code, CFD-RC, was used to calculate and to obtain the

analytic capacity of the micro-cavity for the flowing electrolyte, including the streamline, isoshear-rate, isoconcentration and isovoltage patterns. Further, to fabricate the microstructure of higher surface accurate, higher hardness, lower residual stress and can be duplicated perfectly.

II. THEORETICAL ANALYSIS

As Fig. 1, it illustrates two-dimensional U-type of micro-cavity for micro-electroforming. Parameters a and b are respectively the cavity width and the cavity depth, h is the height of the free electrolyte surface, w is the distance between cavities, the distance between the surface of the cavity cathode and the inlet face of the electrolyte flow was presented by d . About the parameters of geometry scales and electrolyte properties for micro-electroforming of U-Type micro-cavity are shown in Table 1.

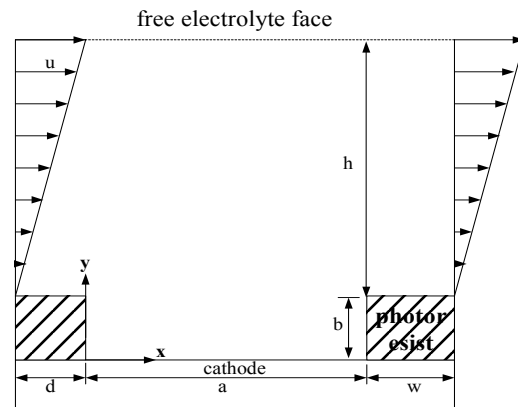


Fig. 1. Physical configuration and coordinate system.

2.1 Assumptions

To simplify the computed model, in this article we used the following assumptions:

Table 1. Geometry scales and electrolyte properties for micro-electroforming

Parameters	Parameter's Values
Cavity width, a	30 μm
Cavity depth, b	10 μm
Free electrolyte surface height, h	40 μm
Distance between the cavities, w	50 μm
Distance between cavity cathode surface & inlet face, d	30 μm
Exchange current density	10 A/m ²
Anode start current density	500 A/m ²
Electrolyte density, ρ	1080 kg/m ³
Electrolyte dynamic viscosity, μ	1.153 $\times 10^{-3}$ kg/m-s
Electrolyte kinematic viscosity, ν	1.07 $\times 10^{-6}$ m ² /s
Electrolyte diffusion coefficient, D	1.67 $\times 10^{-8}$ m ² /s
Electrolyte conductance coefficient, k	38 1/Ohm-m

- (1) Considering the working fluid is electrolyte 0.6 mol/liter CuSO₄ + 1.85 mol/liter H₂SO₄, which the electrolyte with constant (temperature- independent) properties. The temperature of copper electro-deposition bath is 20° C.
- (2) A uniform chemical reaction rate is processing for the electrolyte in the micro-electroforming of U-type micro-cavity, and the micro-electroforming process is steady state and laminar flow.
- (3) The effect of heat diffusion and the compressibility effect in the momentum equation are disregarded.

2.2 Governing equations

The electrochemistry reaction of micro-electroforming is to deposit the metal ion or alloy ion for the microstructure. We relate the

governing equations or the empirical equations in micro-electroforming process to satisfy the behaviors that are presented in the electrolyte flow, electrolyte mass flow and electrolyte voltage distribution.

Electrolyte continuity equation:

$$\nabla \cdot (\rho U) = 0 \quad (1)$$

$U = (u, v)$ is the local velocity vector, velocity components respectively in the X, Y directions, and ρ is the electrolyte density.

Electrolyte momentum equation:

$$(U \cdot \nabla)U = -\frac{1}{\rho} \nabla P + \mu \nabla^2 U \quad (2)$$

where P is the local pressure in the electrolyte flow, and μ is the electrolyte dynamic viscosity.

Convection diffusion equation of electrolyte ion concentration:

$$\nabla \cdot (\rho UC) = \nabla \cdot J \quad (3)$$

where $J = \rho D \nabla C$. Parameters C and D respectively present the ion concentration and the ion diffusion coefficient.

Electrolyte voltage distribution ϕ must satisfy Laplace's equation:

$$\nabla^2 \phi = 0 \quad (4)$$

Using Ohm's law to compute the current density:

$$i = -k \nabla \phi \quad (5)$$

let i be the current density and k be the specific electrolyte conductivity.

2.3 Computation conditions

Linear velocity profile is adopted at the inlet and the outlet (symmetrical) face. The velocity, the concentration, and the voltage are all constant to satisfy the condition of the free electrolyte surface. Both the concentration gradient and voltage gradient are zero because they are

orthogonal to the inert surface of photo-resist. The concentration of copper ion on the surface of the cathode is zero, and the condition of no slip on the photo-resist. The computation conditions are:

$$(du/dy)_{y=0} = \text{const}, v=0, \partial\phi/\partial n = 0, C = C_b$$

at inlet face, (6a)

$$(du/dy)_{y=0} = \text{const}, v=0, \partial\phi/\partial n = 0, \partial C/\partial n = 0$$

at outlet (symmetrical) face, (6b)

$$u = u_\infty, v=0, \phi = \phi_b, C = C_b$$

at free electrolyte surface, (6c)

$$u=v=0, \partial\phi/\partial n = 0, \partial C/\partial n = 0$$

at photo-resist wall, (6d)

$$u=v=0, \phi = 0, C = 0$$

at cathode surface, (6e)

where n is the inward normal coordinate, subscripts b, ∞ denote the bulk quantity and free electrolyte face respectively.

2.4 Calculation of Parameters

To determine the domain of evaluation, the fully developed velocity boundary layer thickness δ , can be represented approximately by Schmidt number Sc following from Incropera and DeWitt [14]:

$$\delta/\delta_c \approx Sc^{1/3} = (\nu/D)^{1/3} \quad (7)$$

where δ, δ_c respectively present the velocity boundary layer thickness and the concentration diffusion boundary layer thickness, ν is the kinematic viscosity and D is the mass diffusion coefficient. The value of $Sc = \nu/D \approx 64$ was calculated by $\nu = 1.07 \times 10^{-6} \text{ m}^2/\text{s}$, $D = 1.67 \times 10^{-8} \text{ m}^2/\text{s}$. Because the concentration diffusion boundary layer thickness δ_c is very thin and let the concentration is C_b at the inlet face, so the concentration diffusion boundary layer thickness δ_c represents the cavity depth b .

Therefore, the velocity boundary layer thickness $\delta = 4b = h$ could be evaluated to satisfy Schmidt number Sc , i.e., the height of the free concentration electrolyte surface and the height of the free velocity electrolyte surface both could be determined. The values of inlet and outlet velocity gradient in the calculated domain are proportional to Pe as shown by Kondo et al. [11]

$$Pe = [\delta^2 (du/dy)_{y=0}] / D \quad (8)$$

The values of inlet and outlet velocity gradient $(du/dy)_{y=0}$ could be calculated by velocity boundary layer thickness $\delta = 4 \times 10^{-5} \text{ m}$ and mass diffusion coefficient $D = 1.67 \times 10^{-8} \text{ m}^2/\text{s}$. Therefore, $Pe = 1.31$ and 41.6 can be respectively obtained $(du/dy)_{y=0} = 13.67$ and 434.2 m/s .

The bulk concentration $C_b = 0.5374 \text{ mol/l}$ was calculated by the corresponding the solute $0.6 \text{ mol/liter CuSO}_4$ and the solution $1.85 \text{ mol/liter H}_2\text{SO}_4$. The value of free electrolyte surface voltage $\phi_\infty = 0.002 \text{ V}$ was calculated by the following corresponding equation

$$\phi_\infty / (\delta + \delta_c) \approx \phi_a / \zeta \quad (9)$$

where the experimental operating voltage of anode ϕ_a is 2 V , and the experimental operating distance between anode and cathode ζ is 5 cm , both are obtained from Yeh [15].

The multi-block grid system is constructed using a commercial code, CFD-RC. By finite volume scheme to obtain the numerical solutions for u, v, C and ϕ , and the numerical methods proposed by Anderson et al. [16] are adopted for discretizing and pressure equation calculation. The mass fraction, Sh/Sh_{\max} , is evaluated on the basic surface concentration distribution of cathode:

$$\begin{aligned} Sh / Sh_{\max} &= (ka / D) / (ka / D)_{\max} \\ &= k / k_{\max} = (\partial C / \partial y)_{y=0} / [(\partial C / \partial y)_{y=0}]_{\max} \end{aligned} \quad (10)$$

where k is the concentration degree at the cathode surface.

The ratio of friction coefficient $C_f / C_{f\max}$ is evaluated by the shear stress distribution τ_s on the hole of the U-type micro-cavity, which is followed as Incropera and DeWitt [14]:

$$\frac{C_f}{C_{f\max}} = \frac{\frac{\tau_s}{\rho V^2 / 2}}{\left(\frac{\tau_s}{\rho V^2 / 2} \right)_{\max}} \quad (11)$$

The fraction of current density I / I_{\max} is also evaluated by the voltage distribution ϕ on the hole of the U-type micro-cavity:

$$I / I_{\max} = \nabla \phi / \nabla \phi_{\max} \quad (12)$$

III. RESULTS AND DISCUSSION

Figure 2 presents the streamline, isoshear-rate, isoconcentration and isovoltage patterns of micro-electroforming in a U-type micro-cavity for $C_b = 0.5374$ mol/l, $\phi_{\infty} = 0.002$ V, $a = 100$ μm and Peclet number $Pe = 1.31$. Figure 2(a) presents the normalized streamline patterns. The streamline value 0.06058 represents the penetrating flow of the electrolyte downstream through the center of the cavity; the nonzero velocity gradient in the horizontal direction near the vertical cavity photo-resist wall caused counter-rotating vortices to appear at the corners of the cavity. Figure 2(b) presents the normalized isoshear-rate patterns, which indicates a symmetrical distribution about the mid-cavity. Near the upstream and downstream sides of the cavity rapidly changes the velocity gradient, yielding the density profile with the highest

isoshear-rates. Figure 2(c) presents the pattern of isoconcentrations normalized to C_b value.

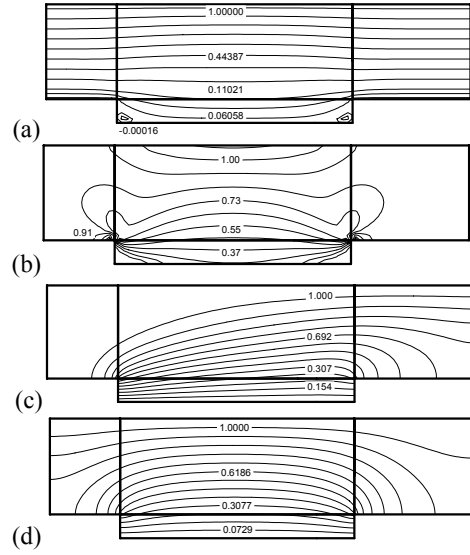


Fig. 2. Patterns for $C_b = 0.5374$ mol/l, $\phi_{\infty} = 0.002$ V, $a = 100$ μm and $Pe = 1.31$, (a) Streamline (b) Isostrain-rate (c) Isoconcentration (d) Isovoltage.

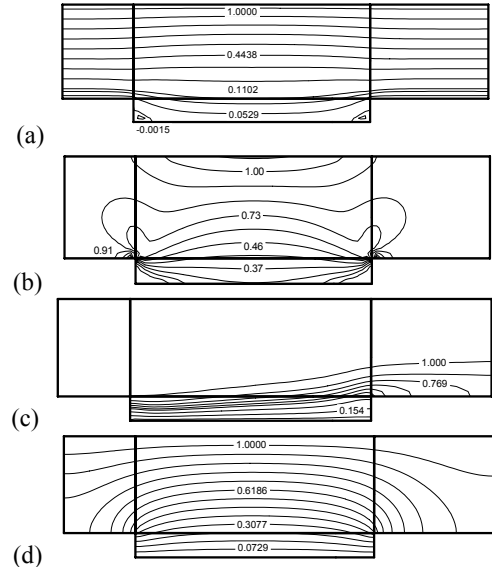


Fig. 3. Patterns for $C_b = 0.5374$ mol/l, $\phi_{\infty} = 0.002$ V, $a = 100$ μm and $Pe = 41.6$, (a) Streamline (b) Isostrain-rate (c) Isoconcentration (d) Isovoltage.

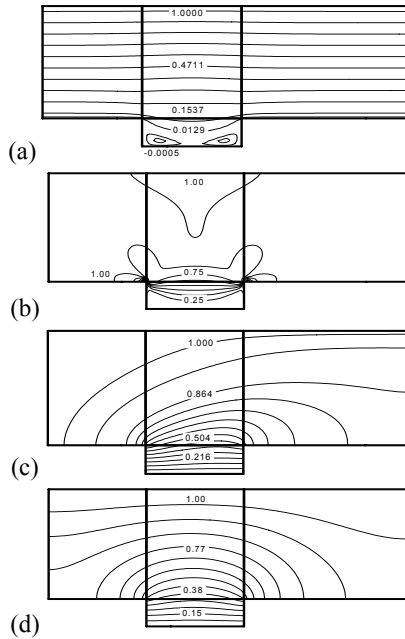


Fig. 4. Patterns for $C_b=0.5374$ mol/l, $\phi_\infty=0.002$ V, $Pe=1.31$ and $a=30$ μm , (a) Streamline (b) Isostrain-rate (c) Isoconcentration (d) Isovoltage.

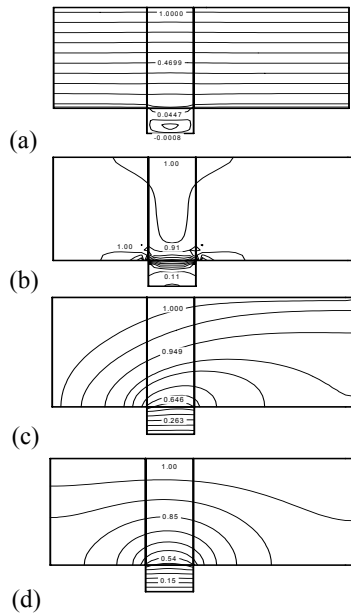


Fig. 5. Patterns for $C_b=0.5374$ mol/l, $\phi_\infty=0.002$ V, $Pe=1.31$ and $a=15$ μm , (a) Streamline (b) Isostrain-rate (c) Isoconcentration (d) Isovoltage.

The upstream vortex is responsible for the capture of more copper ions and the enhancement in local mass transfer, yielding a denser profile. Figure 2(d) presents the iso-voltages normalized to ϕ_∞ , the distribution of which exhibits the phenomenon of camber or round down, and shows that they are almost symmetrical about the mid-cavity.

Figure 3 presents the physical patterns at $C_b=0.5374$ mol/l, $\phi_\infty=0.002$ V, $a=100$ μm and $Pe=41.6$. In relation to the normalized streamline patterns, the value 0.0529 represents penetration flow shown as Fig. 3(a). Figure 3(b) presents the normalized isoshear-rate patterns, which show a maximum value 0.91 near the upstream and downstream sides of the micro-cavity. Figure 3(c) shows that normalized isoconcentration patterns in the U-type micro-cavity at $Pe=41.6$ exhibit a stronger mass convection flow effect, and led to a higher electrolyte concentration density profile than obtained at $Pe=1.31$ (Fig. 2(c)). In Laplace's equation, Eq. (4), the voltage is not coupled to the velocity, so the Pe (velocity gradient) does not influence the voltage distribution in the micro-electroforming process for a U-type micro-cavity. $Pe=1.31$ and 41.6 yield the same normalized isovoltage patterns.

Figure 2 presents some parameters such as bulk concentration C_b , free electrolyte face voltage ϕ_∞ and Pe value. However, for a different micro-cavity width $a=30$ μm , Fig. 4 presents the normalized patterns of the streamline, the isoshear-rate, the isoconcentration, and the isovoltage, similar to those in Fig. 2. In Fig. 4(a), the normalized streamline value 0.0129 represents the penetration flow, and of the electrolyte transport to the surface of the cathode, by

diffusion or convection. The normalized streamline patterns include both counter-rotating vortices at the corners close the upstream and downstream sides of the U-type micro-cavity.

The width of the U-type micro-cavity $a=15\ \mu\text{m}$, as presented in Fig. 5, differs from the width $a=30\ \mu\text{m}$, presented as in Fig. 4. Reduce the width of the micro-cavity enhanced the mass diffusion effect near the up stream and downstream sides, and the mass convection effect near the hole of micro-cavity, forming only a single vortex at the center of the cavity. Therefore, Fig. 5(a) shows that the width $a=15\ \mu\text{m}$ corresponds to a greater penetration flow, 0.0447, than that at $a=30\ \mu\text{m}$, as presented in Fig. 4(a). The normalized streamline patterns in the form of the transition of vortices at both corners, and of the single vortex at the center are observed for cavity widths of 30 to 15 μm . This finding is consistent with the numerical results of Kondo et al. [11]. The other representations of physical phenomena include normalized isoshear-rate, isoconcentration and isovoltage patterns as shown in Figs. 5(b)~5(d), and all of which are similar to in Figs. 4(b)~4(d).

When $C_b=0.5374\ \text{mol/l}$, $\phi_\infty=0.002\ \text{V}$, $a=100\ \mu\text{m}$ and $Pe=1.31\sim 100$, the mass fraction Sh/Sh_{max} on the cathode surface is evaluated to be as illustrated in Fig. 6. The obtained results for $Pe=1.31$ and 46.1 agree excellently with the numerical data of Kondo et al. [11]. The root-mean-squared deviations were under 2.13 %. Therefore, the numerical data of Kondo et al. [11] were obtained to ensure the accuracy of the results herein. At $Pe=1.31$, the copper is transported to the cathode by diffusion flow because more copper ions on the upstream side.

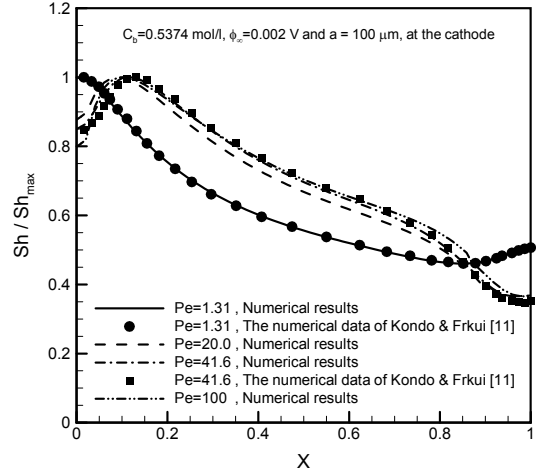


Fig. 6. Mass fraction Sh/Sh_{max} versus X for $C_b=0.5374\ \text{mol/l}$, $\phi_\infty=0.002\ \text{V}$, $a=100\ \mu\text{m}$ and various $Pe=1.31\sim 100$.

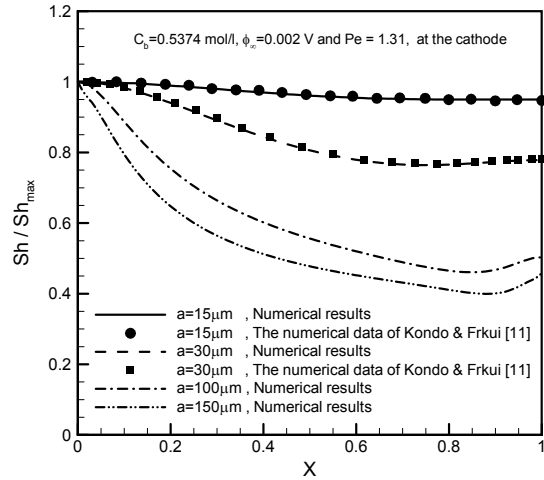


Fig. 7. Mass fraction Sh/Sh_{max} versus X for $C_b=0.5374\ \text{mol/l}$, $\phi_\infty=0.002\ \text{V}$, $Pe=1.31$ and various $a=15\sim 150\ \mu\text{m}$.

Figure 2(c) shows that when the vortex captures more copper ions, the local mass transfer to the cathode is clearly increased, causing the flux to maximal upstream of $X=0$. When a high copper ion concentration causes the penetration flow, the fresh bulk electrolyte first passes through the upstream side, and then moves along the surface of the cathode to the downstream side. During

this process, the copper ions are consumed. When they have reached the downstream side, the local mass transfer to the cathode is again increased to an extent determined by diffusion from the vortex. Therefore, the increase in the flux is at downstream of $X=0.9\sim 1.0$. For $Pe=41.6$, the hump is slightly shifted and appeared at $X=0.16$; this process is mainly governed by both convection of the penetration flow and the effect of the vortices at the corners. Accordingly, the flux gradually decrease toward the downstream side and is flattened by the local resistance at $X=0.95\sim 1.0$. The mass fraction Sh/Sh_{max} in cases $Pe=20\cdot 100$ are similar to that at $Pe=41.6$.

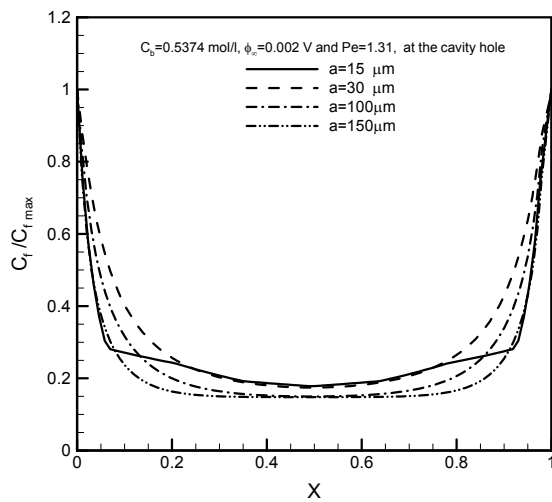


Fig. 8. Friction coefficient ratio $C_f / C_{f,max}$ versus X for $C_b=0.5374$ mol/l, $\phi_\infty=0.002$ V, $Pe=1.31$ and various $a=15\sim 150$ μm .

Figure 7 presents the mass fraction for $C_b=0.5374$ mol/l, $\phi_\infty=0.002$ V, $Pe=1.31$ and $a=15\sim 150$ μm . The Sh/Sh_{max} values on the surface of the cathode are evaluated, and those at $a=15$ and 30 μm agree closely with the numerical data obtained by Kondo et al. [11]. The root-mean-squared deviations were under 1.37 %.

The flux shows that the 30 μm cavity width peaks at about $X=0$. The flux also increases slightly at $X=0.75\sim 1$, in which range the copper ions are captured by the recirculating vortices. The profile at a cavity width of $a=30$ μm resembles those at $a=100$ and 150 μm . However, for a cavity width $a=15$ μm , the profile becomes almost flat and little difference is observed between the upstream and downstream sides.

Figure 8 presents the ratio of friction coefficient $C_f / C_{f,max}$ at the cavity hole for $C_b=0.5374$ mol/l, $\phi_\infty=0.002$ V, $Pe=1.31$, and various cavity widths, $a=15\sim 150$ μm . (The aspect ratios b/a are $2/3\sim 1/15$). These curves are all sagging. The width of the cavity $a=150$ μm (aspect ratio $1/15$) corresponds to a stronger convection effect and a more uniform friction coefficient ratio around the mid-cavity than are observed at $a=15, 30$ and 100 μm . However, at a cavity width $a=15$ μm , the single vortex occupied all of the micro-cavity, causing the diffusion near the upstream and downstream sides of the micro-cavity existing a lower friction coefficient ratio, but, a higher friction coefficient ratio than were associated with convection at $X=0.3\sim 0.7$.

Figure 9 presents the current density fraction I / I_{max} at the cavity hole under the same conditions as shown in Fig. 8. All curves of current density fraction are also displayed in a sagging condition. The current density fraction at a cavity width of $a=15$ μm corresponded to a higher fractional current density because the cathode surface was smaller than at the other values. However, when the width of the cavity was $a=150$ μm , the current density fraction is lower because the cathode surface is larger. The

current density distribution for a cavity width of $a=15\ \mu\text{m}$ is flatter, as is the micro-electroforming layer, than at $a=30, 100$ or $150\ \mu\text{m}$.

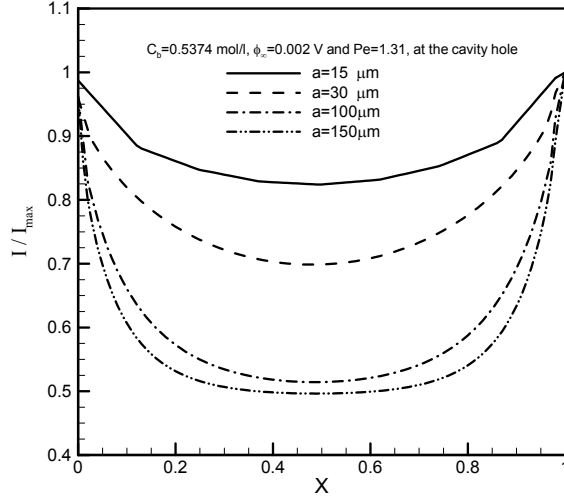


Fig. 9. Current density fraction I/I_{\max} versus X for $C_b=0.5374\ \text{mol/l}$, $\phi_{\infty}=0.002\ \text{V}$, $Pe=1.31$ and various $a=15\sim 150\ \mu\text{m}$.

IV. CONCLUSION

The electrolyte flowing phenomena including the streamline, the isoshear-rate, the isoconcentration, and the isovoltage patterns in the micro-electroforming process are numerically studied. The key findings are as follows.

- (1) With respect to the normalized isoconcentration patterns of the U-type micro-cavity, the larger parameter, such as $Pe=41.6$, corresponds to stronger mass convection and penetration flow effect, and therefore, a higher electrolyte concentration density profile than obtained at $Pe=1.31$.
- (2) For the cavity width $a=15\ \mu\text{m}$, the mass diffusion effect near the upstream and downstream sides was strengthened, and the mass convection effect near the hole of the

micro-cavity was enhanced, so only a single vortex was formed at the center of the micro-cavity. Therefore, normalized streamline patterns are in the form of the transitions of vortices at both corners, and of a single vortex at the center, for cavity width between $a=30$ and $a=15\ \mu\text{m}$.

- (3) The mass fraction Sh/Sh_{\max} on the surface of the cathode is evaluated for different values $Pe=1.31, 41.6$, and various geometry cavity widths $a=15, 30$ and $100\ \mu\text{m}$. The results are all very consistent with the numerical data obtained by Kondo et al. [11].
- (4) The ratio of coefficient fraction $C_f/C_{f\max}$ for various cavity widths $a=15\sim 150\ \mu\text{m}$, these curves are all sagging. At a cavity width $a=150\ \mu\text{m}$, the convection was stronger and the induced the ratio of friction coefficient was higher than those at $a=15, 30$ and $100\ \mu\text{m}$.
- (5) The current density fraction I/I_{\max} for various cavity widths $a=15\sim 150\ \mu\text{m}$ are all also satisfied sagging condition. At the cavity width $a=15\ \mu\text{m}$ the current density was larger, and the cathode smaller than at $a=30, 100$ or $150\ \mu\text{m}$.

NOMENCLATURE

English letters	
a	cavity width (μm)
b	cavity depth (μm)
C	ion concentration (mol/l)
C_b	bulk concentration (mol/l)
C_f	friction coefficient
D	mass diffusion coefficient (m^2/s)
h	free electrolyte surface height (μm)
I	Current density (A/m^2)
k	specific electrolyte conductivity or mass transfer coefficient
P	pressure (N/m^2)
Pe	Peclet Number
Re	Reynolds number
Sc	Schmidt number
Sh	Sherwood number
U	$U=(u, v)$, velocity components in the x, y directions. (m/s)
X	dimensionless distance (x/a)
Greek letters	
δ	velocity boundary layer (μm)
δ_c	concentration boundary layer (μm)
μ	dynamic viscosity ($\text{kg}/\text{s}\cdot\text{m}$)
ν	kinematic viscosity (m^2/s)
ρ	density (kg/m^3)
τ	shear stress (kg/ms^2)
ϕ	voltage (V)
Suffix	
b	bulk value
∞	free electrolyte surface

ACKNOWLEDGEMENT

The authors would like to thank the National Science Council of Taiwan, Republic of China, for financially supporting this research under Contract No. NSC 94-2212-E-268-001.

REFERENCES

- [1] Yang, H., and Kang, S. W., "Improvement of Thickness Uniformity in Nickel Electroforming for the LIGA Process," *J. Machine Tools and Manufacture*, Vol. 40, pp. 1065-1072, 2000.
- [2] Savinell, R. F., Zeller, R. L., and Adams, J. A., "Electrochemically Active Surface Area: Voltammetric Charge Correlation for Ruthenium and Iridium Dioxide Electrodes," *J. Electrochem. Soc.*, Vol. 137, No. 2, pp. 489-494, 1990.
- [3] Tan, H. J. and Chan, K. C., "Numerical Analysis of an Inside-out Tube Inversion Process," *J. of Materials Processing Technology*, Vol. 66, pp. 130-136, 1997.
- [4] Lee, S. L., Lee, Y. F., Chang, M. H., and Lin, J. C., "Pulse Plating Effects During Ni-W Electrodeposition," *Corrosion Prevention & Control*, pp. 71-76, 1999.
- [5] Yin, K. M., Jan, S. L., and Lee, C. C., "Current Pulse with Reverse Plating of Nickel-Iron Alloys in a Sulphate Bath," *Surface and Coatings Technology*, Vol. 88, pp. 219-225, 1996.
- [6] Andricacos, P. C., Tabib, J., and Romankiw, L. T., "Stripping Voltammetry of Nickel-Iron Film Electrodeposited on Platinum Using a Rotating Ring-Disk Electrode," *J. Electrochem. Soc.*, Vol. 135, No. 5, pp. 1172-1174, 1988.
- [7] Yamasaki, T., Schlobmacher, P., Ehrlich, K., and Ogino, Y., "Formation of Amorphous Electrodeposited Ni-W Alloys and Their Nanocrystallization," *Nanostructured Materials*, Vol. 10, No. 3, pp. 375-388, 1998.

- [8] Gould, R. D., and Lopez, M. G., "Electrical Conductivity and Dynamics of Electroforming in Al-SiO_x-Al Thin Film Sandwich Structure," *Thin Solid Films*, Vol. 433, pp. 315-320, 2003.
- [9] Hessami, S., and Tobias, C. W., "A Mathematical Model for Anomalous Codeposition of Nickel-Iron on a Rotating Disk Electrode," *J. Electrochem. Soc.*, Vol. 136, pp. 3611-3616, 1989.
- [10] Pesco, A. M., and Cheh, H. Y., "The Current Distribution within Plated Through-Holes: II. The Effect of Periodic Electrolysis," *J. Electrochem. Soc.*, Vol. 136, No. 2, pp. 408-414, 1989.
- [11] Kondo, K., Fukui, K., Uno, K., and Shinohara, K., "Shape Evolution of Electrodeposited Copper Bumps," *J. Electrochem. Soc.*, Vol. 143, No. 6, pp. 1880-1886, 1996.
- [12] Georgiadou, M., "Modeling Current Density Distribution in Electrochemical Systems," *Electrochemical Acta*, Vol. 48, pp. 4089-4095, 2003.
- [13] Duchanoy, C., and Lapicque, F., "Current Distributions on Patterned Electrodes in Laminar Flow," *Chemical Engineering Science*, Vol. 55, pp. 1115-1126, 2000.
- [14] Incropera, F. P., and DeWitt, D. P., "Fundamentals of Heat and Mass Transfer," 5th ed., John Wiley and Sons, New York, pp. 348-354, 2002.
- [15] Yeh, Y. M., "Fabrication and Characterization Analysis of Ni-Fe Micro Mold by Pulse Electroforming in LIGA-like Technology," Ph. D. dissertation, National Chiao Tung University, Taiwan 300, ROC, 2003.
- [16] Anderson, D. A., Tannehill, J. C., and Pletcher, R. H., Computational Fluid Mechanics and Heat Transfer, McGraw-Hill, New York, pp. 39-46, 1984.